Solar Energy Materials & Solar Cells 95 (2011) 986–991

Contents lists available at ScienceDirect

Solar Energy Materials & Solar Cells

journal homepage: www.elsevier.com/locate/solmat

Influence of laser scribing in the electrical properties of a-Si:H thin film photovoltaic modules

J.J. García-Ballesteros [a,*], I. Torres [b,*], S. Lauzurica [a], D. Canteli [a], J.J. Gandía [b], C. Molpeceres [a]

[a] Centro Láser UPM, Universidad Politécnica de Madrid, Campus Sur UPM, Edificio Tecnológico La Arboleda, Ctra. de Valencia Km 7.3, 28031 Madrid, Spain
[b] Departamento de Energías Renovables, Energía Solar Fotovoltaica, CIEMAT, Avda. Complutense, 22, 28040 Madrid, Spain

ARTICLE INFO

Article history:
Received 9 June 2010
Received in revised form
29 November 2010
Accepted 3 December 2010
Available online 24 December 2010

Keywords:
Monolithic interconnection
Laser ablation
Amorphous silicon thin film module

ABSTRACT

The third (P3) laser patterning step of thin film photovoltaic devices is studied experimentally using a diode pumped solid state laser with 532 nm wavelength and a delay generator. The effect on the electrical characteristics of the devices due to the patterning process is investigated by performing scribes on single, thin-film solar cells. As it is shown, in this type of experiments the inertia in the motion systems or in the scanner controlling the direction of the laser beam plays a critical role in the results. By controlling externally the output of the laser beam it is possible to overcome the inertia and investigate the real effect of the P3 laser scribing on the device electrical characteristics. When the laser scribing conditions are optimized and the inertia in the system is taken care of, the P3 process has very little effect on the device electrical characteristics. Translated to modules this means that by optimizing the P3 process, the decrease in the efficiency found when up-scaling from single cells to modules can be minimized (as far as the P3 process is concerned) to that coming from the removed area.

1. Introduction

Photovoltaic devices based on thin film technology play an important role in green energy generation. The forecasts are that by 2010, thin film modules will reach a capacity of four gigawatt and a market share of 20% [1]. Thin-film modules are still not as efficient per unit area as crystalline silicon modules, however, they possess various advantages that make them an interesting alternative. At the front of these advantages is the fact that thin-film solar is much less expensive to produce and it still has the potential to significantly reduce manufacturing costs. The raw materials required to produce these solar modules are cheaper than the high-grade silicon needed to manufacture crystalline silicon panels. In addition, production costs are also lower thanks to cooler processing temperatures or greater fabrication throughput. This is achieved thanks to faster processing techniques and the possibility of larger area material deposition.

Laser scribing is one of the most important processing steps in the industrial development of thin-film photovoltaic modules. It allows cell isolation and monolithic electrical interconnection over large areas at high speeds. The advantages of laser scribing over other scribing methods is that it can be a highly selective process, with very limited thermal affection of the processed material and with very little debris produced during the process. As it is a relatively new technology, however, the different laser processes involved in the production of solar modules are far from optimized.

In thin-film solar modules based on the superstrate configuration, the different laser scribing processes are as follows [2]. First, the cell's width is initially defined by scribing the transparent conductive oxide that acts as the front electrode so that electrically isolated parallel stripes of TCO are obtained. This process is commonly known as P1 scribe. These scribes are performed either using IR light (1064 nm) by direct writing or by backscribing (sample illuminated through the glass/substrate side) or using UV light (355 nm) by direct scribing [3]. Typically, the width of the P1 scribe ranges from 10 to 30 μm. Following the completion of the P1 scribes, the different thin films that shape the solar cell are deposited. In the case of amorphous silicon (a-Si:H) solar cells, like in the present work, these are deposited typically by Plasma Enhanced Chemical Vapor Deposition (PECVD) in the p–i–n structure (p-doped layer, i-intrinsic layer, n-doped layer). The subsequent laser scribe process consists of the removal of the thin film layers with scribes adjacent to the previously performed P1 scribe and it is known as the P2 scribe. This P2 scribe is performed by backscribing using green light (532 nm) and it allows the serial electrical interconnection of the different cells with the ensuing back contact deposition. Finally, after back contact deposition, a third laser scribe, adjacent to the P2 scribes, is performed by backscribing through the substrate side also using a 532 nm laser. This third scribe, known as P3, completely defines the solar cells and ensures the serial connection of the cells. An example of the three different scribes is shown in Fig. 1.

* Corresponding authors. Tel.: +34 913365541; fax: +34 913365534.
E-mail addresses: Juanjo.garcia-ballesteros.ramirez@upm.es (J.J. García-Ballesteros), ignacio.torres@ciemat.es (I. Torres).

0927-0248/$ - see front matter © 2010 Elsevier B.V. All rights reserved.
doi:10.1016/j.solmat.2010.12.007

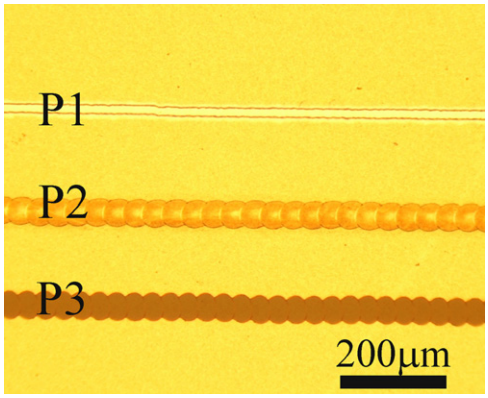

Fig. 1. Microscopic image of P1, P2 and P3 scribes in an a-Si:H thin film photovoltaic device.

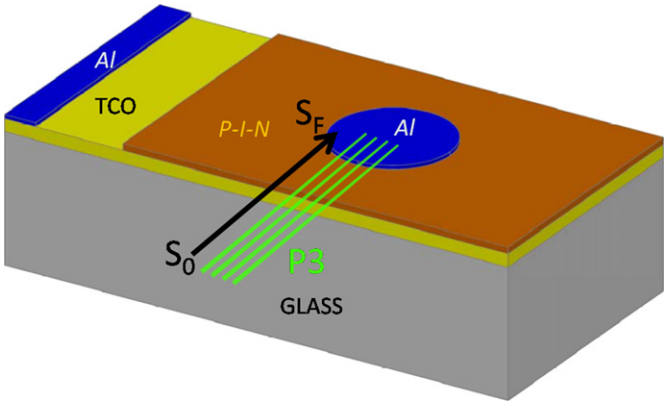

Fig. 2. Sketch of the sample structure and laser patterning used to investigate the influence of the P3 scribing process in the devices electrical characteristics.

This work focuses on the P3 laser scribing process with the peculiarity that it has been done in single solar cells. By evaluating it in single solar cells rather than in finished modules it is possible to isolate its effect on the device characteristics since the P1 and P2 scribes are omitted. Furthermore, it is a much faster way for evaluating different process parameters and the overall quality of the P3 scribe. Optimum laser power and overlapping area are easier to evaluate with this method. To study the effect of the P3 scribe length, several scribes can be done in the same cell. However, as will be shown in this work, the high speed motion systems needed for precision laser scribing plays an important role in this experiment. They can be responsible for the electrical losses observed after scribing the solar cells. If this is dealt with properly, it can be seen that the P3 scribes have very little effect on the electrical characteristics of the processed solar cells.

2. Experimental

2.1. Sample preparation

a-Si:H thin film solar cells with a p–i–n structure were deposited onto SnO_2:F (Asahi-U type)/glass substrate in a dual chamber PECVD reactor at 13.56 MHz from the decomposition of silane (SiH_4). Tri-methyl boron ($B(CH_3)_3$) and phosphine (PH_3) were used as the doping gases for the p and n layers, respectively. The cell total thickness was estimated to be around (400 nm). An aluminum back contact was thermally evaporated, limiting the area of the cells to 1 cm^2. Typical total area efficiency of these cells was ~8%.

2.2. Laser scribing

Laser scribing has been performed using a diode pumped solid state laser (Nd:YVO_4) from Spectra Physics. The system includes an electro-mechanical shutter and it can operate with a repetition rate within the range 15–100 kHz with pulse widths of 15 ns in TEM 00 operation mode. The fundamental frequency of the laser is 1064 nm (IR). However, the system also includes a second harmonic module, which effectively doubles the frequency to 532 nm (green light).

The laser beam is focused on the sample surface by an optical system constituted of three mirrors, two telescope expanders that can reduce/increase the size of the spots and a digital scanner (HurryScan II, SCANLAB) for 532 nm light with a focal of 250 mm and working distance of 383 mm. This produces a typical usable square image field of 155 × 155 mm^2 with a scanning velocity of 3 mm/s to 10 m/s. Part positioning is assured by X, Y stages, which are servomotor driven with linear position encoder (resolution of 0.1 μm in each axis). Overall precision in the XY working area is about 1 μm. An additional linear axis (*Z*-axis) is used to bring the part to the laser focus. Finally, the laser beam can be controlled by means of a DG645 digital delay generator that can output arbitrary delays from 0 to 2000 s with 5 ps resolution and typical RMS jitter of 12 ps.

To study the effect of the P3 scribes on the electrical characteristics of solar cells, the scribes need to end (or to start) within the back contact electrode, otherwise what are obtained are two different cells completely isolated (see Fig. 2). But in doing so, the accuracy of the interconnection system is very important. The inertia in the braking and acceleration of the motion systems (XY stages or digital scanner), when making scribes at typical speeds of 1 m/s, can be quite significant even if very accurate precision, low-inertia systems plus the perfect synchronies and control of the laser beam as the ones used here are employed. In fact, stopping the XY stages in a controllable way within an electrode of 1 cm^2 as the one used here has proved to be very difficult because of the higher mechanical and kinetic loads. Therefore, the length of the scribes has been controlled using only the scanners. To avoid the possible influence of the inertia in the scanner, a delay generator can be used so that it is possible to program a stop to the laser emission before the end of the programmed scribe.

After each backscribing process, the samples were subjected to an ultrasonic bath in ethanol and were nitrogen-dried, to avoid the presence of loose flakes or debris of the back contact that could lead to errors in the measurements.

2.3. Measurements and characterization techniques

The quality of the laser scribes and the ablation profiles were studied using optical microscopy (Olympus PMG3, Olympus SZ-CTV) and confocal laser scanning microscopy (Leica DCM 3D). In confocal microscopy techniques, 3D images are obtained by moving the focus plane and acquiring single images that can be put together building up a three-dimensional stack of images to be digitally processed. Using a 150 × magnification objective, vertical resolutions of 2 nm can be achieved. In addition, SEM and EDX micrographs are included for a better description of the morphology and to obtain qualitative information about the selective-ablation processes.

To study the effect of the laser scribes in the performance of the solar cells, the current–voltage characteristics (*J–V*) have been measured in dark and under calibrated 100 mW/cm^2 AM1.5G irradiance. The main photovoltaic parameters i.e. short-circuit

current density (J_{sc}), open-circuit voltage (V_{oc}), fill factor (FF) and efficiency (η) have been obtained in the usual way. The dark J–V characteristics have been numerically fitted to the general diode equation (see Fig. 3 for equivalent circuit)

$$J_0 = J_s(e^{(V-AJR_s/nV_T)}-1)+\frac{V-AJR_s}{R_{sh}} \quad (1)$$

In Eq. (1), J_0 is the measured dark current, J_s is the saturation current, V is the applied voltage, A is the cell area, R_s is the series resistance, n is the diode ideality factor, $V_T=q/KT$ and R_{sh} is the shunt resistance. As will be shown, any effect in the solar cell dark J–V curves after P3 scribing is primarily assimilated by the R_{sh} value. Hence, this value will be used to assess the effect of P3 laser scribing on the electrical characteristics.

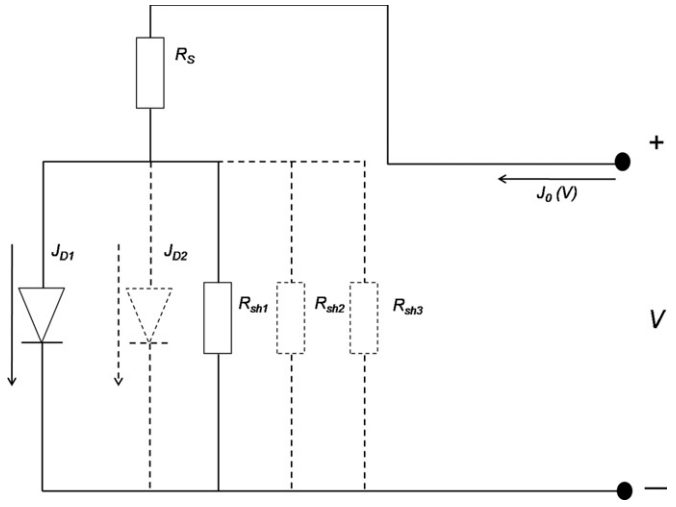

Fig. 3. Equivalent circuit of the pin solar cell measured in dark conditions from which Eq. (1) is derived.

3. Results and discussion

3.1. Optical characterization of back contact patterning

Two of the most important parameters that need to be optimized for a successful P3 scribe are laser power density and pulse overlap [4]. When the cell is irradiated, the laser pulse energy is absorbed at the *TCO*/p–i–n interface. If the increase in temperature due to the energy absorption reaches local thermal strain, melting and vaporization (ablation) of the thin films can occur "sweeping away" the metallic back reflector as well. The extra energy above the ablation threshold goes into the material as heat, causing thermal damage to the surrounding area. This explosive removal of the thin films results in a scribe quality that depends on the mechanical properties of the back contact, on the laser beam power density and on the pulse overlap.

The laser beam profile of the laser system used in this work is Gaussian. Therefore the spatial distribution of the energy fluence is given by

$$E(r) = \int_{-\infty}^{\infty} dtI(r,t) = E_0 \exp(-r^2/\rho^2) \quad (2)$$

Since the energy distribution or the energy fluence is given by the spatial (r) and temporal (ρ) radius, the power density used for the line groove can affect the quality of the scribes in different ways.

If the power density is very low it can lead to an incomplete removal of the thin films resulting in poor levels of isolation on all the scribes processes [5]. If instead, a very high power density is used, the TCO can be heavily damaged by the ablation process increasing the sheet resistance and deteriorating the device overall electrical characteristics. An example of the damaged induced to the TCO by using very high power density is shown in Fig. 4A. In addition, a higher thermal damage to the thin films is expected, which in turn can create regions with a higher defect density and induce crystallization [6] of the silicon thin films Furthermore, owing to the Gaussian nature of the power distribution, energy excess can produce thermal effects like inducing a bulging of the back contact (Fig. 4B) due to the Gaussians queues.

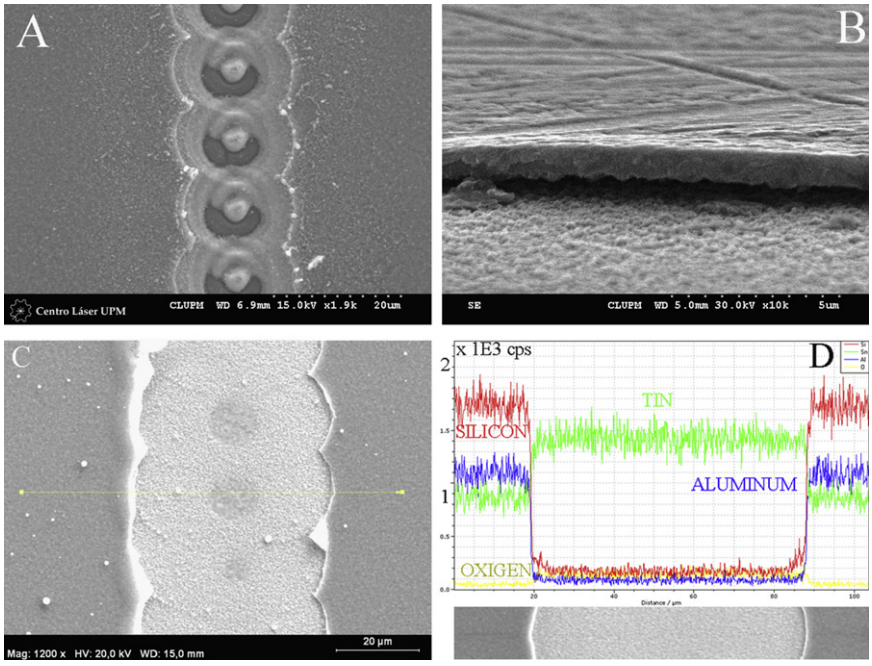

Fig. 4. SEM micrograph of a P3 scribe showing damage done to the TCO (A), bulging of the back contact (B) and metal flake formation (C) due to non-optimized conditions. (D) Shows an EDX micrograph of an optimized P3 scribe.

Pulse overlap is determined by the scribing speed, once the laser repetition rate is fixed according to the power of the laser. If pulse overlap is not optimized flakes or tongues of un-removed back contact reflector are created, which can give rise to potential short circuits paths in the finished device [4]. This is shown in Fig. 4C where the unwanted flakes are clearly seen along the edges of the scribe.

Once the power density and pulse overlap are optimized, the thin films are perfectly removed as confirmed from EDX images (Fig. 4D) with no damage to the TCO or metal flakes along the edges. It is possible to correct the profile of a Gaussian distribution through the homogenization of the laser beam and therefore facilitate the laser patterning of P3 interconnection.

In the present work, the scribes need to be stopped within the back electrode reflector as explained in the experimental section. If the scribe is stopped being used by the scanner or by the motion systems, what is typically obtained is something like the scribe shown in Fig. 5A. As can be observed, the system is very accurate and it can be brought to a stop in distances of only 50 μm. However, since the laser continues emitting pulses at the same frequency, the overlap of the last pulses (those within the breaking distance) increases. As a result, flakes and therefore potential short-circuits are created.

If, on the other hand, the output of the laser is controlled in conjunction with a delay generator, the scribes are controlled to a greater accuracy. An example of these scribes can be seen in Fig. 5B. A close-up of the end of these scribes (Fig. 6) reveals that with this method the overlap is maintained until the last stop and hence, the scribe comes out perfectly clean of flakes. It is clear then, that to study the effect of P3 scribes in single solar cells without taking any extra precaution can lead to some erroneous results. In the following section, the electrical characteristics of cells treated with P3 scribes performed with and without a delay generator are presented.

3.2. Electrical characterization of the patterned solar cells

The electrical characteristics (dark *J–V* curves) after back contact patterning are shown in Fig. 7 for both methods of stopping the scribe, within the back electrode. The characteristics of a cell, where the scribe was finished, using only the scanner are those of Fig. 7A (cell PF8), whereas Fig. 7B (cell PH1) corresponds to a cell where the delay generator was used.

It is clear that the electrical characteristics of the cell where the scribe had stopped using the scanner worsen drastically with each scribe, whereas using the delay generator leaves them practically unchanged. By fitting the *J–V* curves to Eq. (1) it can be seen that the only real change in the diode characteristics after each scribe occurs in R_{sh}. The series resistance, the saturation current or the diode ideality factor remain practically constant after each of the scribing processes. In the present example, cell PF8 suffers a decrease in R_{sh} from 2.4×10^6 to $5.3 \times 10^3\ \Omega\ cm^2$ after the cell has been modified with 12 P3 scribes.

The same behavior of cell PF8 has been observed by others authors [4]. In their work, the observed worsening of the electrical characteristics was attributed to an accumulative effect of the total length of the P3 scribes. They concluded that as the total length increases, so does the heat affected zone in the vicinity close to the patterned area. As it has already been shown [6] that a recrystallization of the material occurs, which could lead to an increase in the defect density (dislocation density, structural defects, diffusion of the dopands in that area, etc.) causing an increase in the dark current. However, in the examples presented here these observations do not explain the results. In the case of the cell PF8, the total length of the P3 scribes amounts to only 2.759 cm after 12 P3 scribes whereas in the case of the cell PH1 the total length of the P3 scribes reaches 13.1 cm after 24 P3 scribes. Nevertheless, the deterioration of cell PF8 is remarkable and practically non-existent in cell PH1.

To further investigate the relationship between the total accumulated length of the P3 scribes and the observed deterioration of the *J–V* curves when the scribes had finished using the scanner, different cells were treated with the same number of P3 scribes but having different length. Cell PF8 was treated with P3 scribes that were substantially shorter than those done in cell PF3. After each P3 scribe, the cells' JV characteristics were measured and R_{sh} was calculated. In Fig. 8A it is shown how the calculated R_{sh} for

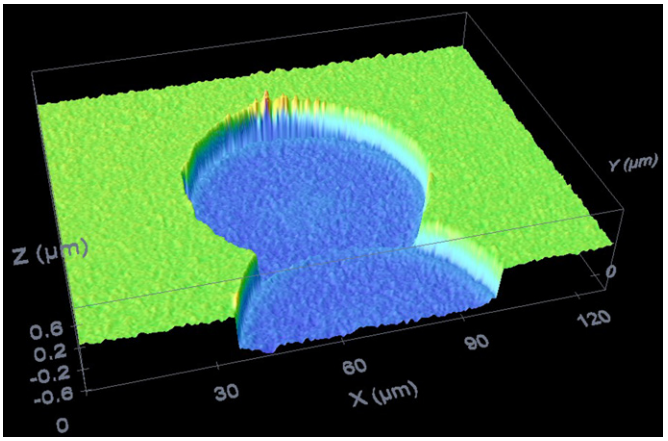

Fig. 6. 3D Confocal profile of a P3 scribe done employing the delay generator (see Fig. 5B).

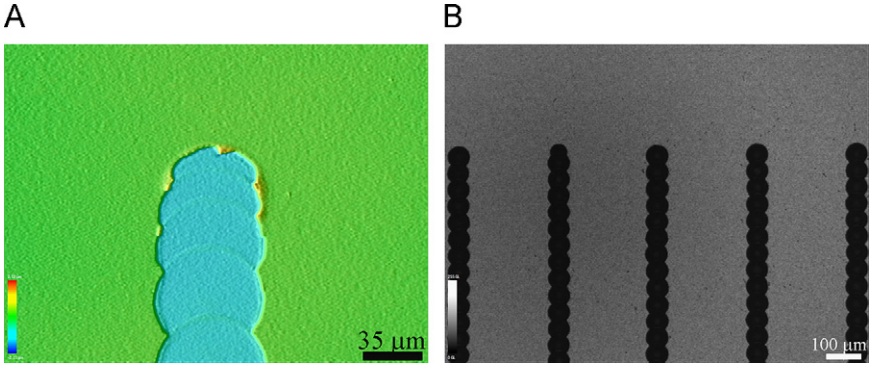

Fig. 5. (A) Confocal microscopy image of a P3 scribe finished within the back contact by controlling the beam with the scanner and (B) optical microscopy image of several P3 scribes finished within the back contact by controlling the output of the beam with a delay generator.

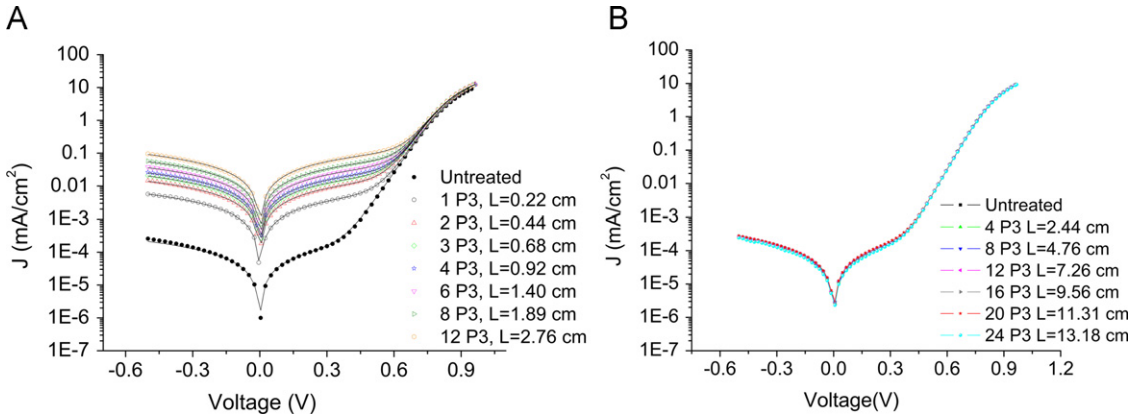

Fig. 7. Dark *J–V* characteristics of cells treated with P3 scribes. (A) Corresponds to cell PF8, where the P3 scribes were controlled using only the scanner. Cell PH1 is shown in (B), and the scribes were controlled using the delay generator. The lines show the fits to Eq. (1).

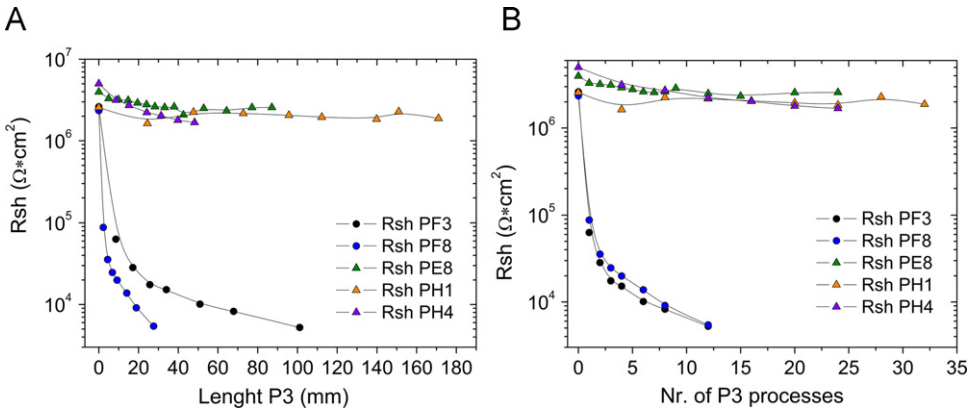

Fig. 8. (A) Shunt resistance R_{sh} vs the total accumulated length in the P3 scribe and (B) R_{sh} vs the number of P3 scribes. The scribes in cells PF3 and PF8 were controlled using only the scanner, whereas in cells PE8, PH4 and PH1 the delay generator was used.

both cells changes when plotted against the total accumulated length of the P3 scribe. If there was a direct relationship between the decrease in R_{sh} and the total accumulated length of the P3 scribe one would expect the same or similar R_{sh} value for a similar total accumulated length for both cells. However, R_{sh} changes differently in both cells with the P3 total length and hence it is not possible to directly relate the total length with the deterioration in the R_{sh} value.

On the other hand, if the same data is plotted not against the total length but against the number of P3 scribes (Fig. 8B) both cells behave similarly and the decrease in R_{sh} after each scribe is practically the same. These results suggest that the total length of the P3 scribe is not responsible for the deterioration in the *J–V* characteristics of the cells. If the same experiment is performed but using the delay generator to stop the scribes instead (cells PE8, PH4 and PH1 in Fig. 8A and B) the value of R_{sh} remains practically unchanged even for a total length of the P3 scribes above 16 cm and 32 different P3 processes. Hence, the observed changes in cells PF3 and PF8 has to be related with the different way of stopping the scribe and not the scribe itself, i.e., the deterioration in the *J–V* curves is due to the formation of flaws or metal flakes within the last 3–4 laser spots. The defects formed in the heat affected zones caused by the P3 scribes are not significantly changing the device's electrical characteristics; otherwise its effect would also be observed when the delay generator is used.

This study has been performed and validated in 22 different cells coming from 5 different depositions and hence, the results cannot be ascribed to peculiarities of the cells formerly shown. Fig. 9 shows, as an overview, the ratio of the original calculated R_{sh} value to the

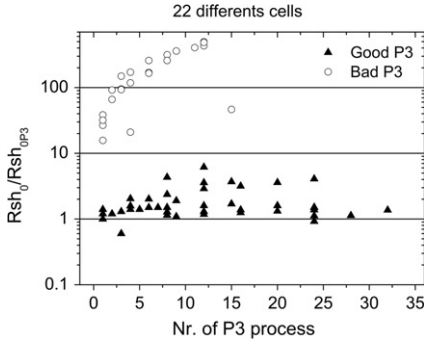

Fig. 9. Ratio of the original calculated R_{sh} value to the value after the different P3 process vs the number of P3 processes. Open circles correspond to cells with P3 scribes performed using only the scanner; filled triangles correspond to cells with P3 scribes performed using the delay generator.

value after the different P3 process plotted against the number of processes. When the delay generator is used and the scribes are free of flakes, the change in R_{sh} is always less than one order of magnitude. On the other hand, if the scribe is finished by stopping the motion systems, the R_{sh} value rapidly increases with the number of P3 processes.

The changes observed in the electrical characteristics under illumination also depend on how the P3 process is performed. However, the effect is relatively soft if compared to the effect in the dark *J–V* characteristics. When the P3 scribe is done using the delay generator, the characteristics under illumination remain completely

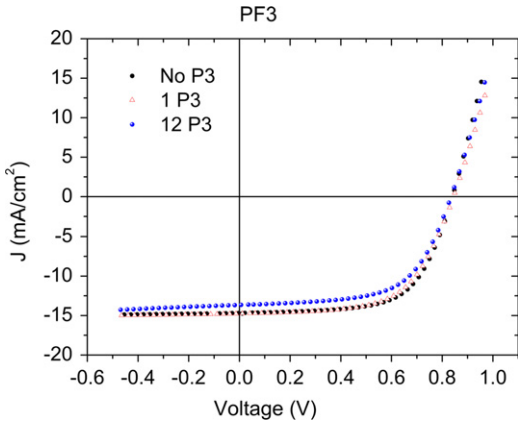

Fig. 10. *J–V* characteristics measured under illumination of cell PF3 before and after 1 and 12 P3 scribes. The scribes were performed using only the scanner to stop the scribes within the back electrode. If the delay generator is also used no deterioration in the *J–V* characteristics of the cells is observed.

unchanged. If the P3 scribes are done using only the scanner, the characteristics do suffer from a slight worsening as can be seen in Fig. 10 for a cell measured after 1 and 12 P3 scribes. As shown, J_{sc} and FF suffer a slight decrease, going from 14.7 to 13.7 mA/cm^2 and from 0.64 to 0.61 after 12 P3, respectively.

This worsening in the electrical characteristics of the cells cannot be translated to complete modules since the scribes connect different cells, without stopping in the middle of the back contact. Hence, there is no influence of the inertia carried by the scanner and motion systems on beginning and ending the scribes, since its effect occurs outside the module. Therefore, if the scribing parameters are optimized, the modules should only be affected by the removal of active area, and not by possible effects induced by the P3 laser process itself. However, the vibrations and mechanical, kinetic and inertial loads of the encoders, servo motors, etc. could have similar harmful consequences in the electrical parameters.

4. Conclusions

The effect of the third laser patterning step used in the fabrication of thin film solar modules has been investigated. To isolate the effect of this step from the P1 and P2 steps, this study has been performed in single solar cells, in which the P3 scribes are accomplished so that the end of the scribes lie within the back contact. Since the laser beam covers the cell at speeds typically of m/s, the inertia when stopping the scribe can be considerable. As shown through different imaging techniques the end of the scribes suffer from the formation of metal flakes due to the variation in the overlap of consecutive spots within the stopping distance. The devices see a continuous worsening of the dark electrical characteristics after each scribe, mainly manifested by a decrease in the shunt resistance. Both the effects: the formation of metal flakes and the decrease in R_{sh} appear to be intimately related. A direct relationship between the decrease in R_{sh} and the total accumulated length of the P3 scribes cannot be established; however, it is shown that the worsening in R_{sh} is related with the number of scribing processes. If, on the other hand, the output of the laser beam is controlled externally with a delay generator (a time delay is introduced between the end of the programmed scribe and the laser output), the scribes can be done with the same spot overlap maintained until the end (start) of the scribe. In this case, the devices electrical characteristics remain practically unchanged even after 32 scribes (total accumulated length of 17 cm). Hence, the observed decrease in R_{sh} is a consequence of the metal flakes formation and not the scribing process itself. This is important because it shows how it is possible to perform P3 scribes in modules without altering the electrical characteristics. The decrease in efficiency usually found when going from single cells to complete modules coming from the P3 laser scribes can be reduced to the effect of the active area removed if all other parameters are optimized.

Acknowledgements

The authors would like to thank José Domingo Santos and Nieves González for the device preparation. Partial financial support was provided by the Spanish Ministry of Education under CLASICO (ENE2007-67742-004-01/ALT) and PSE-MICROSIL (PSE-120000-2007-7).

References

[1] 〈http://www.epia.org/〉.
[2] J. Bovatsek, A. Tamhankar, R.S. Patel, N.M. Bulgakova, J. Bonse, Thin film removal mechanisms in ns-laser processing of photovoltaic materials, Thin Solid Films 518 (10) 2897–2904, doi:10.1016/j.tsf.2009.10.135.
[3] C. Molpeceres, S. Lauzurica, J.J. García-Ballesteros, M. Morales, G. Guadaño, M. Colina, I. Sánchez-Aniorte, J.L. Ocaña, J.J. Gandía, F. Villar, O. Nos, J. Bertomeu, UV laser selective ablation of photovoltaic materials for monolithic interconnection of devices based on a-Si:H, in: Proceedings of the 23rd European Photovoltaic Solar Energy Conference, © 2008-WIP, volume I, pp. 2438–2442, ISBN 3-936338-24-8.
[4] S. Haas, A. Gordijn, H. Stiebig, High speed laser processing for monolithical series connection of silicon thin-film modules, Progress in Photovoltaics 16 (2008) 195–203.
[5] M. Vetter, J.P. Borrajo, J. Andreu, Fabrication of very large 2.6 m × 2.2 m amorphous silicon solar modules on glass, in: A.G. Loureiro, N.S. Iglesias, M.A.A. Rodriguez, E.C. Figueroa (Eds.), Proceedings of the 2009 Spanish Conference on Electron Devices, IEEE, New York, 2009, pp. 406–409.
[6] C. Molpeceres, M. Colina, M. Holgado, M. Morales, I. Sánchez-Aniorte, S. Lauzurica, J.J. García-Ballesteros, J.L. Ocaña. Optical characterization of the heat-affected zone in laser patterning of thin film a-Si:H, Proceedings of SPIE, the International Society for Optical Engineering, 7202 (2009), 72020R-72020R10, ISSN 0277-786X doi:10.1117/12.809514.